

PAPER • OPEN ACCESS

Functionalised hexagonal-domain graphene for position-sensitive photodetectors

To cite this article: Adolfo De Sanctis *et al* 2017 *Nanotechnology* **28** 124004

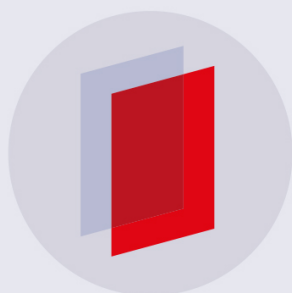
View the [article online](#) for updates and enhancements.

Related content

- [Facile electrochemical transfer of large-area single crystal epitaxial graphene from Ir\(1 1 1\)](#)
Line Koefoed, Mikkel Kongsfelt, Søren Ulstrup *et al*.
- [Advances in graphene-based optoelectronics, plasmonics and photonics](#)
Bich Ha Nguyen and Van Hieu Nguyen
- [Reducing the Schottky barrier between few-layer MoTe₂ and gold](#)
Dianyu Qi, Qixing Wang, Cheng Han *et al*.

Recent citations

- [Intrinsic Plasmon–Phonon Interactions in Highly Doped Graphene: A Near-Field Imaging Study](#)
Francisco J. Bezares *et al*
- [Reduced graphene oxide-germanium quantum dot nanocomposite: electronic, optical and magnetic properties](#)
Tabitha A Amollo *et al*
- [Focus on graphene and related materials](#)
Filippo Giubileo *et al*



IOP | ebooks™

Bringing you innovative digital publishing with leading voices to create your essential collection of books in STEM research.

Start exploring the collection - download the first chapter of every title for free.

Functionalised hexagonal-domain graphene for position-sensitive photodetectors

Adolfo De Sanctis, Matthew D Barnes, Iddo Amit, Monica F Craciun and Saverio Russo

Centre for Graphene Science, College of Engineering, Mathematics and Physical Sciences, University of Exeter, Exeter EX4 4QF, United Kingdom

E-mail: s.russo@exeter.ac.uk

Received 31 October 2016, revised 16 December 2016

Accepted for publication 7 February 2017

Published 24 February 2017



CrossMark

Abstract

Graphene's unique photoresponse has been largely used in a multitude of optoelectronics applications ranging from broadband photodetectors to wave-guide modulators. In this work we extend the range of applications to position-sensitive photodetectors (PSDs) using FeCl₃-intercalated hexagonal domains of graphene grown by atmospheric pressure chemical vapour deposition (APCVD). The FeCl₃-based chemical functionalisation of APCVD graphene crystals is affected by the presence of wrinkles and results in a non-uniform doping of the graphene layers. This doping profile creates multiple p-p⁺ photoactive junctions which show a linear and bipolar photoresponse with respect to the position of a focused light spot, which is ideal for the realization of a PSD. Our study paves the way towards the fabrication of flexible and transparent PSDs that could be embedded in smart textile and wearable electronics.

Keywords: APCVD, graphene, intercalation, photodetector, Raman, position-sensitive

(Some figures may appear in colour only in the online journal)

1. Introduction

The isolation of a single layer of graphene [1] has triggered an immense response in the scientific community in the past decade [2, 3]. Both the exceptional electrical and optical properties of this material have been studied in detail and exploited in many areas of pure and applied research. In particular, its broadband absorption and field effect tunability make graphene an excellent platform for optoelectronic devices [4]. The breadth of such devices includes high-responsivity [5] and high-speed [6] broadband photodetectors (PDs), wave-guide coupling [7] and transparent and flexible electrodes [8]. The photoresponse of graphene PDs has been investigated with many techniques, though so far no reports have been made of its application in position sensitive detectors (PSDs). Such devices traditionally consist of a semiconductor (Si or Ge) junction with four contacts, which

exploits the *lateral photoeffect* [9], that is the photovoltage generated at the junction plane in the presence of localized illumination, in addition to the conventional photovoltage effect that is formed across the junction. This effect has been extensively studied in the past [10, 11] and it is at the base of PSDs used currently in many applications, such as: laser alignment, motion control, automation and scanning probe microscopy. The detection of focused x-rays via field-effect in a graphene transistor has been shown [12] though no other uses of graphene for PSDs in the UV-visible-NIR spectral range have been reported.

In this work we present the first chemical functionalisation of multilayer hexagonal domains of graphene grown by atmospheric pressure chemical vapour deposition (APCVD) [13] and demonstrate its use as an all-graphene PSD. Pristine graphene presents fundamental limitations in optoelectronic applications, such as a low intrinsic conductivity and the lack of bandgap. Chemical functionalisation [14] has been employed in the past years to overcome such limitations providing researchers with a stable and robust platform, thanks to the opening of an energy bandgap [15] or an increase in the conductivity of graphene. Amongst the



Original content from this work may be used under the terms of the [Creative Commons Attribution 3.0 licence](https://creativecommons.org/licenses/by/3.0/). Any further distribution of this work must maintain attribution to the author(s) and the title of the work, journal citation and DOI.

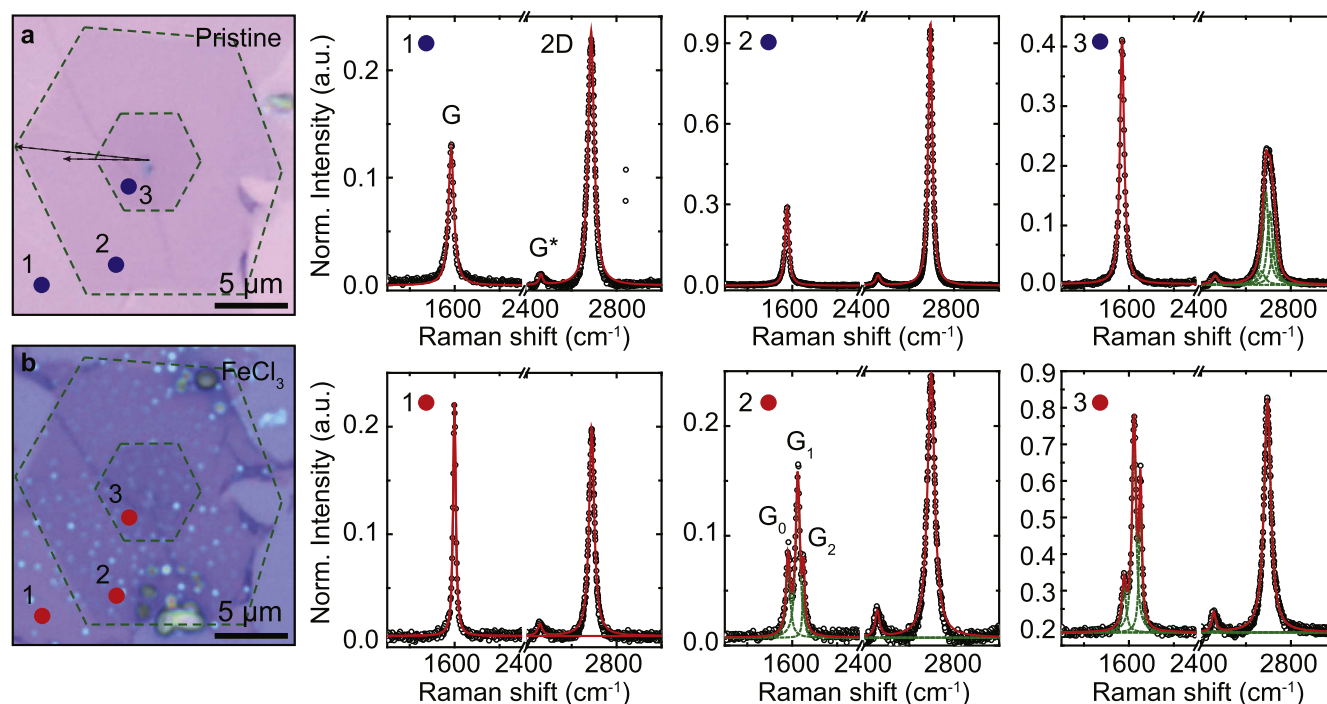


Figure 1. (a) Optical micrograph (left) and Raman spectra (right) of pristine APCVD graphene hexagonal crystals on three different locations: (1) first crystal on substrate, (2) second layer grown on the first, (3) third layer. Dashed lines indicate the twisting of the hexagonal crystals. (b) Optical micrograph and Raman spectra of the same crystals after intercalation with FeCl₃. Raman spectra are normalized to the height of the 1-TO mode of Si at 520 cm⁻¹.

different forms of functionalisation, intercalation with FeCl₃ [16], is used to induce strong p-type doping in the graphene layers, making it particularly suitable for use as transparent electrodes [17, 18]. It has been recently reported that FeCl₃-intercalated graphene, employed in a light emitting device, gives an enhanced light emission of 60% compared to standard graphene electrodes and up to 40% enhancement compared to commercial conductive polymers [8] while having an unprecedented stability in ambient conditions [19]. Here we intercalate multilayer (two to three layers) hexagonal crystals of graphene with FeCl₃ and characterize them using Raman spectroscopy and atomic force microscopy (AFM). After intercalation, we fabricate a multi-terminal device and characterize it using scanning photocurrent mapping (SPCM) [20]. The formation of wrinkles in the as-grown graphene is associated with the observed photoresponse of the device, in agreement with the charge density distribution measured across the device, using Raman spectroscopy mapping. Several junctions between regions of high (p⁺) and low (p) doping are observed and the position of such p-p⁺ junctions correlates well with the observed photocurrent (PC). Furthermore, the photoresponse scales linearly with the position of the excitation source and changes sign at the centre of the p-p⁺ junctions. The observed linearity and bipolarity make our device suitable for position-sensitive detection of focused light. Our findings, combined with the high stability of FeCl₃-intercalated graphene [19] and the ability to grow millimetre-sized single crystals [13], fill a technological gap in the inventory of all-graphene devices and open a route towards

the fabrication of flexible PSDs for a multitude of novel applications.

2. Experimental methods

2.1. Graphene growth and intercalation

Multilayer hexagonal domains of graphene were grown on copper by APCVD [21] using a melting/re-solidification pre-treatment step to reduce nucleation density and increase domain size. Growth was carried out at ~1075 °C using diluted CH₄ (1000 ppm) as the carbon precursor and a high H₂/CH₄ (50/25 sccm) to aid multilayer formation. The crystals were then transferred to highly doped Si substrate capped with 285 nm thermal SiO₂ using PMMA-supported electrochemical delamination [22, 23]. The delamination step was performed using a 0.5 M NaCl solution and glassy carbon anode at 0.5 A, followed by rinsing in de-ionized water.

The intercalation with FeCl₃ was performed using a previously reported vapour phase method in vacuum [16]. More specifically, graphene on SiO₂/Si and anhydrous FeCl₃ (Sigma-Aldrich, powder, ≥99.99% trace metals basis) are placed in a glass tube of a multi-zone resistive heated furnace. The glass tube is sealed after evacuating it to a pressure < 10⁻⁵. Hence the sample is heated at a temperature of 360 °C and the FeCl₃ at the sublimation temperature of 315 °C for 12 h. The furnace is then left to cool and the sample removed.

After the intercalation, samples were washed in acetone and isopropyl alcohol in order to remove FeCl₃ residues from

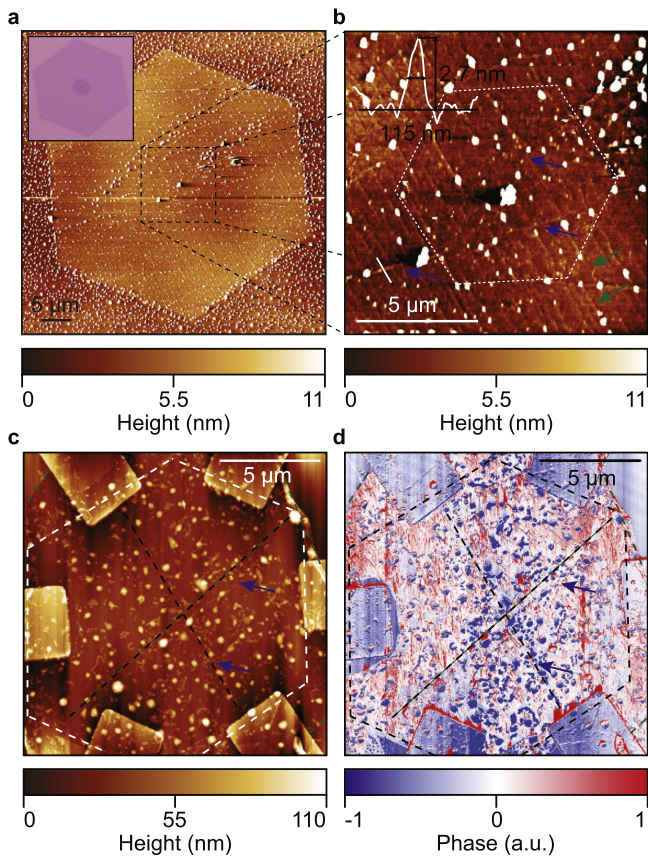


Figure 2. (a) AFM topography of a pristine APCVD graphene hexagonal crystal after transferring onto Si/SiO₂ substrate. Inset: optical micrograph of the same crystal. (b) High resolution AFM topography of the central area. Blue and green arrows indicate wrinkles. Inset: profile of a wrinkle, height 2.7 nm and width 115 nm. (c) AFM topography of a graphene hexagonal crystal after intercalation with FeCl₃ and fabrication of a multi-terminal photodetector device (see main text). (d) Tapping phase image of the same device. Dashed lines as in figure 3, blue arrows indicate the residual wrinkles. White dots are PMMA residues from the transfer process (see main text).

the substrate. The quality of the growth, the transfer and the degree of intercalation with FeCl₃ was assessed via optical inspection, AFM and micro-Raman spectroscopy. All measurements were performed in atmosphere and at room temperature. Raman spectra were acquired using a *Renishaw* spectrometer, with 532 nm excitation laser with incident power density of 0.3–1 MW cm⁻² through a $\times 50$ objective lens. The scattered light was dispersed by a 2400 g mm⁻¹ grating and recorded by a CCD with 5 s integration time. Raman maps were acquired with the same setup performing a raster scan of the area in 0.5 μ m steps. AFM topography and phase image were acquired with a *Bruker Innova* AFM system, operating in the ‘tapping’ mode using a sharp (radius of curvature < 10 nm) highly doped silicon tip from *Nanosensors* with a nominal resonance frequency of 330 kHz.

2.2. Devices fabrication and characterization

Multi-terminal PDs were fabricated on the same substrates. Metal contacts were defined via electron-beam lithography

using 300 nm thick PMMA as resist, followed by electron-beam evaporation of Ti/Au (5/50 nm) and lift-off in acetone. The sample was then contacted to the chip carrier by mean of wedge bonding using 20 μ m thick gold wire. SPCM was performed using a custom-built setup [20]: a laser beam ($\lambda_{in} = 375$ nm) was focused on the sample by a $\times 50$ objective lens to a ~ 260 nm spot diameter. The sample was mounted on a motorized microscope stage and raster-scanned under the laser beam. The photoresponse of the device was measured in short-circuit configuration for each point, producing a two-dimensional map of the photogenerated current (see also figure 3(a)). The light of the laser was modulated at a frequency of 33.25 Hz and the current measured via an *Ametek 7270* DSP Lock-in amplifier locked at the same frequency.

3. Results and discussion

3.1. Functionalization of graphene single crystals

Figure 1(a) shows the optical micrographs and Raman spectra of a pristine, as-transferred, multi-layer hexagonal domain of graphene grown by APCVD. Each layer grows in a stacked sequence, where the multi-layers appear at the centre of the first single-layer indicating that they share the same nucleation site [24]. The Raman spectrum of the first layer (1) shows the two main features of graphene: the G peak at ~ 1585 cm⁻¹, originating from the resonant E_{2g} mode and the 2D peak at ~ 2700 cm⁻¹, originating from the double-resonant A_{1g} mode [25]. The shape of the 2D band, a single Lorentzian peak, and intensity ratio $I_{2D}/I_G \sim 1.9$ confirms the single-layer nature of the graphene. The spectrum of the second layer (2) shows the same features but with a ratio $I_{2D}/I_G \sim 3.36$, which deviates from the expected ratio for two AB-stacked graphene layers [26]. This is due to the rotation of the crystallographic axes with respect to the underlying layer, producing an effective decoupling of the two stacked layers [21, 27]. The third layer (3) is slightly twisted with respect to the second, as shown by optical inspection, and the spectrum shows a 2D band that can be fitted with the convolution of four Lorentzian peaks, which is characteristic of twisted bilayer graphene with a twist angle $< 3^\circ$ [21, 28]. These observations are common to all the crystals we examined.

Functionalization with FeCl₃ strongly affects the electronic characteristics of graphene [14, 17]. FeCl₃ intercalates between the layers of graphene forming a stacked sequence of graphene/intercalant/graphene [29]. Charge transfer to the FeCl₃ layer causes p-doping of the graphene [16], which results in the non-adiabatic removal of the Kohn anomaly at the Γ point and the consequent stiffening of the E_{2g} mode of graphene [30]. This stiffening is observed in the upshift of the G peak [31–33] in the Raman spectrum of graphene. Figure 1(b) presents the optical micrograph and the Raman spectra of the intercalated flake. Optically we can see each hexagonal crystal, with a change in contrast due to the presence of FeCl₃. The Raman spectra are acquired in the same locations as in figure 1(a). The first layer (1) shows an upshift

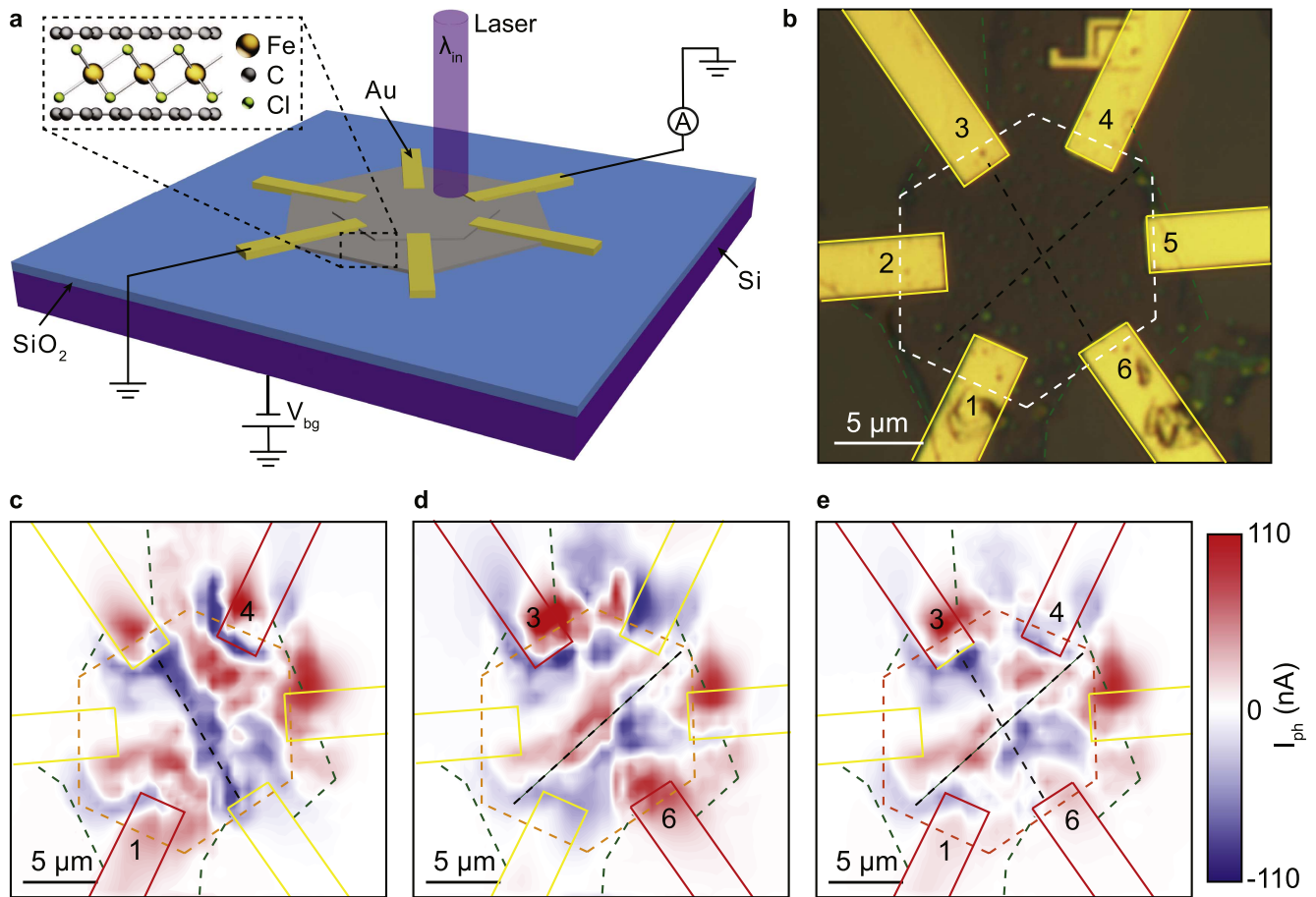


Figure 3. (a) Schematic of the multi-terminal device and measuring geometry. A laser of incident wavelength λ_{in} is scanned across the surface and the electrical response is measured in short-circuit configuration, producing a 2D map of the generated photocurrent. Inset: layer structure of FeCl₃-intercalated graphene. (b) Optical micrograph of the device. (c) SPCM map with contacts 3 and 6 connected. (d) SPCM map with terminals 1 and 4. (e) Sum of the SPCM maps shown in panels (c) and (d). Dashed green lines mark the first graphene layer while dashed hexagons (white and orange) mark the second. Dashed black lines indicate the regions in the flake where I_{ph} reverses sign.

of the position of the G peak to 1600 cm^{-1} and an increase in the height ($I_{2D}/I_G \sim 0.92$), both indicating small doping of the graphene [33]. The second (2) and third (3) layers show the same characteristic spectra. We observe a split of the G band into three peaks, each corresponding to different doping levels: the G_0 -peak is the signature of pristine graphene; the G_1 -peak is given by a graphene layer in contact with one FeCl₃ layer (stage-2) and the G_2 -peak is given by one layer of graphene sandwiched between two FeCl₃ layers (stage-1). The 2D-band is also indicative of the effective decoupling of the graphene layers by the intercalant, as can be seen in the third spectrum, the multi-peak structure is reduced to a single Lorentzian peak, signature of the loss of stacking order within the graphene layers. The peaks related to the FeCl₃ molecules lie at significant lower energies ($100\text{--}400\text{ cm}^{-1}$) [34], therefore they do not interfere with the modes of graphene. These results confirm the successful intercalation of single crystal APCVD graphene with FeCl₃.

To evaluate the quality of our intercalated APCVD graphene we used AFM. Figures 2(a) and (b) show the topography image of a pristine single crystal, with a second layer grown at the centre, as seen optically (inset). Here we observe a series of parallel wrinkles (green arrows), which match the

topography of the re-solidified copper used as metal catalyst during the growth. More interestingly, we observe larger wrinkles running in the perpendicular direction with respect to the first ones, originating from the centre of the crystal (blue arrows) and ending close to the middle of the hexagon's side. Wrinkles in APCVD graphene have been previously reported [23, 35] to form during the cooling stage due to the different thermal expansion coefficients of graphene and copper. In the same images, residues of PMMA from the transfer process appear as white dots, as previously reported [36].

Intercalation with FeCl₃ changes the topography of the single crystals. Figures 2(c) and (d) show the AFM topography and phase images of an intercalated single crystal. In this case the image was acquired after fabrication of metal contacts. Focusing on the topographic features we immediately notice the absence of the substrate-related wrinkles, while a number of bubble-like structures are still present and the cross-directional wrinkles can still be seen (blue arrows). The disappearance of small wrinkles is attributed to the intercalation process: by separating the graphene layers, the intercalant allows them to relax. The AFM phase image can readily distinguish between different materials, as it

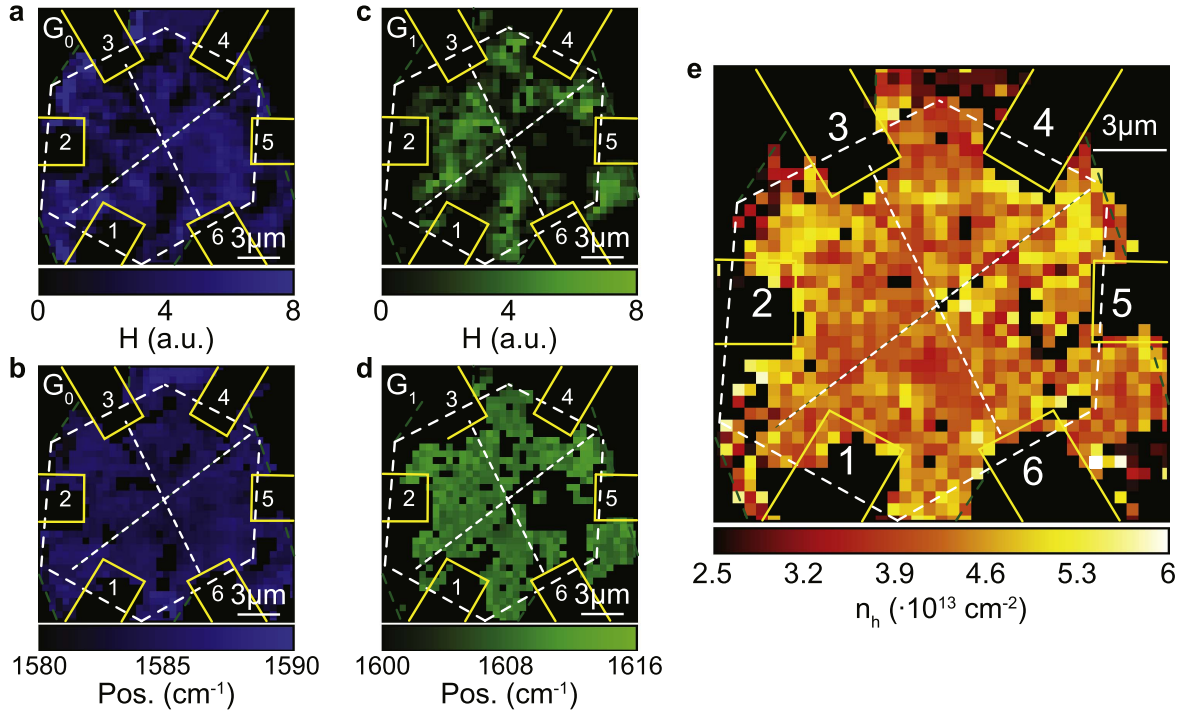


Figure 4. Raman maps of the the multi-terminal device. (a) G_0 peak height. (b) G_0 peak position. (c) G_1 peak height. (d) G_1 peak position. (e) Total intercalation-induced hole concentration in the crystal. Solid and dashed lines as in figure 3.

represents the phase lag between the tip excitation signal and its motion that is due to the (viscoelastic) damping properties of the sample [37]. In figure 2(d) it can be seen that the bubble-like structures observed in topography show a clear phase contrast. Since no annealing was performed after the transfer of graphene from the copper substrate, the PMMA residues observed before intercalation are still present during the process. The distribution and density is, indeed, comparable with what is observed in the pristine crystal, suggesting that those structures are caused by the contamination of graphene, arising from the transfer process. Clustering of FeCl_3 around these areas can contribute to the observed contrast. The presence of wrinkles, in particular along the crossed lines which extends from the centre of the crystal to the sides of the hexagon, is still clearly visible.

3.2. APCVD graphene PDs

Having successfully intercalated single crystal multi-layer graphene, we proceed to study its optoelectronic properties. Figure 3(a) shows a schematic representation of a multi-terminal device. Here the contacts have been positioned in parallel to the sides of the top-layer hexagon, as shown in the optical micrograph (figure 3(b)). The resistance across two opposing pair of contacts, namely 1–4 and 3–6 in figures 3(a) and (b), was $R_{1-4} = 660 \pm 2 \Omega$ and $R_{3-6} = 670 \pm 2 \Omega$, in agreement with previous measurements [16]. The photoresponse of the device was characterized using SPCM, employing different pairs of contacts. Figures 3(c) and (d) show the SPCM maps acquired with two different pairs of contacts (1–4 and 3–6, respectively). Both SPCM maps show PC I_{ph} being generated across the whole device, with a net

change in sign appearing at the centre of it, in the direction orthogonal to the contacts. The dashed black lines in panels (c) and (d) mark the position of the maxima of the PC. Measuring across both pair of contacts and summing the two signals we obtain a SPCM map which displays a clear four-fold symmetry of the PC, as shown in figure 3(e) where the black dashed lines are the same as in panels c and d. Superimposing these lines, extrapolated from the SPCM map, onto the AFM maps of the same device, shown in figures 2(c) and (d), we see that they match with the observed crossed wrinkles in the graphene crystal.

The role of grain boundaries and wrinkles in graphene-based PDs has been studied via near-field PC nanoscopy, where the presence of grain boundaries was associated with a reversal in the sign of the PC while enhanced PC was observed in the presence of wrinkles [38]. The growth of hexagonal domains by APCVD is known to give high-quality, defect-free, graphene. Therefore, we do not expect any grain boundaries to be present across the device. All our observations point towards the fact that the observed PC is related to the intercalation spatial inhomogeneity, and thus to the doping inhomogeneity, of the graphene crystals. The presence of wrinkles is likely to create clusters of FeCl_3 , increasing the level of doping in those regions, while sign reversal is related to a sharp change in doping, forming a p–p⁺ junction in the highly doped graphene. These junctions can therefore act as photoactive centres giving the observed photoresponse for the overall device.

To confirm these hypotheses we acquired a Raman map of the device (see methods). In figures 4(a)–(d) we report the fit of Lorentzian peaks to the G-band region, as previously discussed (see figure 1(b)). Figures 4(a) and (b) show the

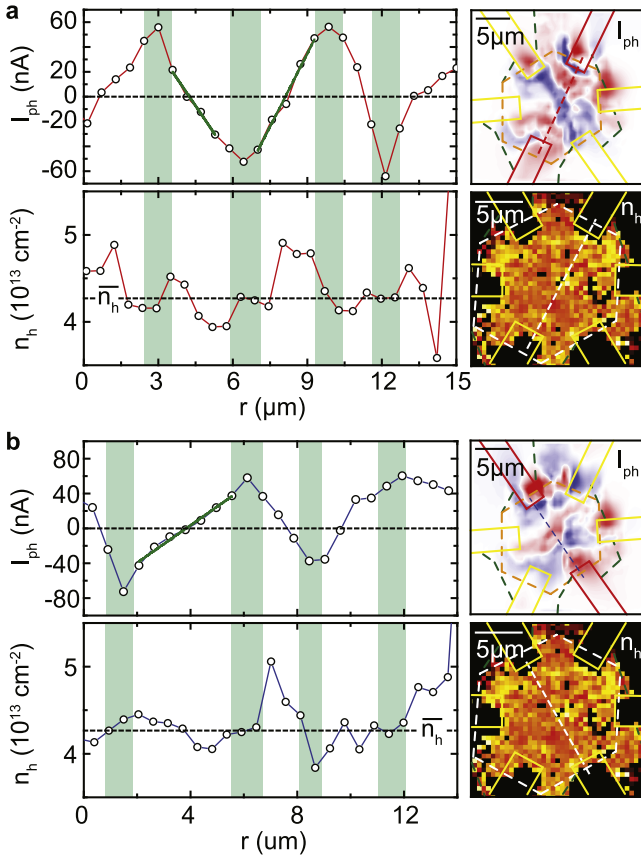


Figure 5. (a) Line profiles of photocurrent I_{ph} (top) and total hole density n_h (bottom) taken along the dashed lines shown in the right panels, with contacts 3 and 6 connected. (b) Same line profiles as in (a) with contacts 1 and 4. Green solid lines mark the linear regions, green-shaded areas mark the maxima and minima of the PC and the corresponding hole density. \bar{n}_h is the log-normal mean value of the reported data.

height and position of the G_0 peak, respectively, while the G_1 band is shown in figures 4(c) and (d). The presence of a blueshifted G_0 peak agrees very well with the boundaries of the crystal and indicates areas with partial intercalation of FeCl_3 within the graphene layers. We observe that the G_1 peak height decreases significantly across a sign reversal in PC (the cross-shaped structure). This decrease in height is also accompanied by a redshift of the G_1 peak, from $\sim 1612 \text{ cm}^{-1}$ to $\sim 1605 \text{ cm}^{-1}$, in the same region, as shown in figure 4(d). We used the model developed by Lazzeri *et al* [30] to extrapolate the total density of holes in doped graphene from the position of the G-band peaks. It has been shown that this model gives an estimation of the charge density within 10% of the values extrapolated with transport techniques [17]. The results are shown in figure 4(e): here we see that a gradient of charge density is present along the two lines determined by the PC maps, confirming our hypotheses.

The PMMA residues observed in figures 2(a)–(d) do not contribute to the observed doping, and therefore to the photoresponse, since the charge transfer due to residual PMMA ($\sim 10^{11} \text{ cm}^{-2}$, see [36]) is negligible compared to the high

level of doping induced by the intercalation with FeCl_3 ($> 4 \times 10^{13} \text{ cm}^{-2}$).

3.3. Towards graphene-based PSDs

The unique PC distribution, with a four-fold symmetry, observed in our device (figure 3(e)), can be used for position-sensitive applications. Commercial PSDs exploit the photo-voltage generated parallel to a semiconductor junction in the presence of local illumination [9]. This effect has been extensively studied in the past [10, 11] and is characterized by a bipolar linear photoresponse as function of illumination position. Figures 5(a)–(c) show the line profiles extrapolated from the SPCM maps in figures 3(c) and (d), while figures 5(b)–(d) show the same line profiles acquired on the charge density n_h maps in figure 4(e). The mean value of the log-normal distribution of n_h ($\bar{n}_h = (4.27 \pm 0.02) \times 10^{13} \text{ cm}^{-2}$) separates values $n_h < \bar{n}_h$ (low doping, p regions) and $n_h > \bar{n}_h$ (high doping, p^+ regions). We can clearly see that the extremes of I_{ph} are located where n_h crosses \bar{n}_h , i.e. in the presence of a p – p^+ junction. At the same time, bipolar linear regions are present (green lines), where the PC changes sign at the centre of the photoactive junction. This behaviour is very similar to what is observed in a lateral photoactive junction [9]. In this case the junction is formed between areas of different doping in the functionalised graphene, induced by the inhomogeneity of the FeCl_3 intercalation driven by the wrinkles in the pristine APCVD single crystals. Therefore, exploiting a multi-terminal geometry as the one adopted here, it is possible to use these linear regions to determine the position of a focused light spot on the device.

4. Conclusion

In conclusion, we have shown that multilayer APCVD-grown hexagonal crystals of graphene can be intercalated with FeCl_3 and used as PSDs. We characterized the degree of intercalation and the resulting doping of graphene, showing the formation of multiple p – p^+ junctions associated with the presence of wrinkles in the pristine APCVD crystals. We then characterized the photoresponse of a multi-terminal device showing a strong spatial correlation between the observed PC and the p – p^+ junctions. The photoresponse is found to be a linear function of the laser spot position and changes sign at the centre of each junction. This behaviour, combined with a four-fold pattern in the spatially resolved PC, makes these devices ideal candidates for position sensitive detection of focused light. Furthermore, all measurements have been repeated after ~ 11 months exposure of the device to environmental conditions, showing no change in the photoresponse, in agreement with the previously reported stability of this material [19]. These findings pave the way to additional functionality in graphene-based optoelectronic devices and open a new route towards flexible, lightweight, transparent and highly stable PSDs, with possible employment in smart textiles and wearable electronics [39].

Acknowledgments

S Russo and M F Craciun acknowledge financial support from EPSRC (Grant no. EP/J000396/1, EP/K017160/1, EP/K010050/1, EPG036101/1, EP/M001024/1, EPM002438/1), from Royal Society international Exchanges Scheme 2016/R1, from European Commission (FP7-ICT-2013-613024-GRASP) and from the Leverhulme Trust (grant title ‘Quantum Drums’ and ‘Room temperature quantum electronics’). I Amit received funding from the People Programme (Marie Curie Actions) of the European Union’s Eighth Framework Programme Horizon 2020 under REA grant agreement number 701704.

Author contributions

ADeS and MDB conceived the experiment. ADeS conducted the intercalation of the graphene, fabricated and measured the devices, analysed the data and wrote the manuscript. MDB grew and transferred the APCVD graphene. IA performed the AFM measurements. MFC and SR supervised the project. All authors contributed to the interpretation of the results and editing of the manuscript.

Competing financial interest

The authors declare no competing financial interest.

References

- [1] Novoselov K S, Geim A K, Morozov S V, Jiang D, Zhang Y, Dubonos S V, Grigorieva I V and Firsov A A 2004 Electric field effect in atomically thin carbon films *Science* **306** 666–9
- [2] Geim A K and Novoselov K S 2007 The rise of graphene *Nat. Mater.* **6** 183–91
- [3] Geim A K 2009 Graphene: status and prospects *Science* **324** 1530–4
- [4] Koppens F H L, Mueller T, Avouris P, Ferrari A C, Vitiello M S and Polini M 2014 Photodetectors based on graphene, other two-dimensional materials and hybrid systems *Nat. Nano* **9** 780–93
- [5] Liu C-H, Chang Y-C, Norris T B and Zhong Z 2014 Graphene photodetectors with ultra-broadband and high responsivity at room temperature *Nat. Nano* **9** 273–8
- [6] Mueller T, Xia F and Avouris P 2010 Graphene photodetectors for high-speed optical communications *Nat. Photon.* **4** 297–301
- [7] Wang X, Cheng Z, Xu K, Tsang H K and Xu J-B 2013 High-responsivity graphene/silicon-heterostructure waveguide photodetectors *Nat. Photon.* **7** 888–91
- [8] Alonso E T, Karkera G, Jones G F, Craciun M F and Russo S 2016 Homogeneously bright, flexible, and foldable lighting devices with functionalized graphene electrodes *ACS Appl. Mater. Interfaces* **8** 16541–5
- [9] Wallmark J T 1957 A new semiconductor photocell using lateral photoeffect *Proc. IRE* **45** 474–83
- [10] Lucovsky G 1960 Photoeffects in nonuniformly irradiated p–n junctions *J. Appl. Phys.* **31** 1088–95
- [11] Carr T G, Richmond J C and Wagner R G 1970 Position-sensitive schottky barrier photodiodes: time-dependent signals and background saturation effects *IEEE Trans. Electron Devices* **17** 507–13
- [12] Cazalas E, Sarker B K, Moore M E, Childres I, Chen Y P and Jovanovic I 2015 Position sensitivity of graphene field effect transistors to x-rays *Appl. Phys. Lett.* **106** 223503
- [13] Mohsin A *et al* 2013 Synthesis of millimeter-size hexagon-shaped graphene single crystals on resolidified copper *ACS Nano* **7** 8924–31
- [14] Craciun M F, Khrapach I, Barnes M D and Russo S 2013 Properties and applications of chemically functionalized graphene *J. Phys.: Condens. Matter* **25** 423201
- [15] Martins S E, Withers F, Dubois M, Craciun M F and Russo S 2013 Tuning the transport gap of functionalized graphene via electron beam irradiation *New J. Phys.* **15** 033024
- [16] Khrapach I, Withers F, Bointon T H, Polyushkin D K, Barnes W L, Russo S and Craciun M F 2012 Novel highly conductive and transparent graphene-based conductors *Adv. Mater.* **24** 2844–9
- [17] Bointon T H, Jones G F, De Sanctis A, Hill-Pearce R, Craciun M F and Russo S 2015 Large-area functionalized CVD graphene for work function matched transparent electrodes *Sci. Rep.* **5** 16464
- [18] Bointon T H, Craciun M F and Russo S 2015 Is graphene a good transparent electrode for photovoltaics and display applications? *IET Circuits Devices Syst.* **9** 403–12
- [19] Wehenkel D J, Bointon T H, Booth T, Boggild P, Craciun M F and Russo S 2015 Unforeseen high temperature and humidity stability of FeCl₃ intercalated few layer graphene *Sci. Rep.* **5** 7609
- [20] De Sanctis A, Jones G F, Townsend N J, Craciun M F and Russo S 2016 An integrated and multi-purpose microscope for the characterization of atomically thin optoelectronic devices arXiv: [1609.07514](https://arxiv.org/abs/1609.07514)
- [21] He R, Chung T-F, Delaney C, Keiser C, Jauregui L A, Shand P M, Chancey C C, Wang Y, Bao J and Chen Y P 2013 Observation of low energy raman modes in twisted bilayer graphene *Nano Lett.* **13** 3594–601
- [22] Wang Y, Zheng Y, Xu X, Dubuisson E, Bao Q, Lu J and Loh K P 2011 Electrochemical delamination of CVD-grown graphene film: toward the recyclable use of copper catalyst *ACS Nano* **5** 9927–33
- [23] Gao L *et al* 2012 Repeated growth and bubbling transfer of graphene with millimetre-size single-crystal grains using platinum *Nat. Commun.* **3** 699
- [24] Mohsin A *et al* 2013 Synthesis of millimeter-size hexagon-shaped graphene single crystals on resolidified copper *ACS Nano* **7** 8924–31
- [25] Ferrari A C and Basko D M 2013 Raman spectroscopy as a versatile tool for studying the properties of graphene *Nat. Nano* **8** 235–46
- [26] Malard L M, Pimenta M A, Dresselhaus G and Dresselhaus M S 2009 Raman spectroscopy in graphene *Phys. Rep.* **473** 51–87
- [27] Lenski D R and Fuhrer M S 2011 Raman and optical characterization of multilayer turbostratic graphene grown via chemical vapor deposition *J. Appl. Phys.* **110** 013720
- [28] Cao Y, Luo J Y, Fatemi V, Fang S, Sanchez-Yamagishi J D, Watanabe K, Taniguchi T, Kaxiras E and Jarillo-Herrero P 2016 Superlattice-induced insulating states and valley-protected orbits in twisted bilayer graphene *Phys. Rev. Lett.* **117** 116804
- [29] Thomas J M, Millward G R, Schlögl R F and Boehm H P 1980 Direct imaging of a graphite intercalate: evidence of interpenetration of ‘stages’ in graphite: ferric chloride *Mater. Res. Bull.* **15** 671–6
- [30] Lazzeri M and Mauri F 2006 Nonadiabatic Kohn anomaly in a doped graphene monolayer *Phys. Rev. Lett.* **97** 266407
- [31] Zhao W, Tan P H, Liu J and Ferrari A C 2011 Intercalation of few-layer graphite flakes with FeCl₃: Raman determination

- of fermi level, layer by layer decoupling, and stability *J. Am. Chem. Soc.* **133** 5941–6
- [32] Zhan D, Sun L, Ni Z H, Liu L, Fan X F, Wang Y, Yu T, Lam Y M, Huang W and Shen Z X 2010 FeCl₃-based few-layer graphene intercalation compounds: single linear dispersion electronic band structure and strong charge transfer doping *Adv. Funct. Mater.* **20** 3504–9
- [33] Das A *et al* 2008 Monitoring dopants by raman scattering in an electrochemically top-gated graphene transistor *Nat. Nano* **3** 210–5
- [34] Caswell N and Solin S A 1978 Vibrational excitations of pure FeCl₃ and graphite intercalated with ferric chloride *Solid State Commun.* **27** 961–7
- [35] Wu Y A, Fan Y, Speller S, Creeth G L, Sadowski J T, He K, Robertson A W, Allen C S and Warner J H 2012 Large single crystals of graphene on melted copper using chemical vapor deposition *ACS Nano* **6** 5010–7
- [36] Pirkle A, Chan J, Venugopal A, Hinojos D, Magnuson C W, McDonnell S, Colombo L, Vogel E M, Ruoff R S and Wallace R M 2011 The effect of chemical residues on the physical and electrical properties of chemical vapor deposited graphene transferred to SiO₂ *Appl. Phys. Lett.* **99** 122108
- [37] García R and Perez R 2002 Dynamic atomic force microscopy methods *Surf. Sci. Rep.* **47** 197–301
- [38] Woessner A *et al* 2016 Near-field photocurrent nanoscopy on bare and encapsulated graphene *Nat. Commun.* **7** 10783
- [39] Neves A I S, Bointon T H, Melo L V, Russo S, de Schrijver I, Craciun M F and Alves H 2015 Transparent conductive graphene textile fibers *Sci. Rep.* **5** 9866